

Optimal Planning for Heterogeneous Smart Radio Environments

Reza Agahzadeh Ayoubi* *Member, IEEE*, Eugenio Moro*, *Member, IEEE*,
Marouan Mizmizi, *Member, IEEE*, Dario Tagliaferri, *Member, IEEE*,
Ilario Filippini, *Senior Member, IEEE*, Umberto Spagnolini, *Senior Member, IEEE*

Abstract—Smart Radio Environment (SRE) is a central paradigm in 6G and beyond, where integrating SRE components into the network planning process enables optimized performance for high-frequency Radio Access Network (RAN). This paper presents a comprehensive planning framework utilizing realistic urban scenarios and precise channel models to analyze diverse SRE components, including Reconfigurable Intelligent Surface (RIS), Network-Controlled Repeater (NCR), and advanced technologies like simultaneous transmitting and reflecting RIS (STAR RIS) and trisectoral NCR (3SNCR). We propose two optimization methods—full coverage minimum cost (FCMC) and maximum budget-constrained coverage (MBCC)—that address key cost and coverage objectives by considering both physical characteristics and scalable costs of each component, influenced by factors such as NCR amplification gain and RIS dimensions. Extensive numerical results demonstrate the significant impact of these models in enhancing network planning efficiency for high-density urban environments.

Index Terms—Smart radio environment, reflective intelligent surfaces, network-controlled repeaters, radio access network, heterogeneous SRE, STAR RIS

I. INTRODUCTION

The ever-growing demand for data envisioned for 6G as well as the evolution of communication technologies necessitates the exploration of new frequency bands, in the centimeter-wave (6 – 24 GHz), a.k.a. mid-band, and millimeter wave (mmW) spectrum portions (24 – 100 GHz). A notable factor of these bands is their harsh propagation characteristics and the high sensitivity to link blockage, which limit the network coverage. Therefore, looking beyond 5G, the future of Radio Access Network (RAN) architectures hinges on two pivotal advancements. On one side, Integrated-Access-and-Backhauling (IAB) allows to mitigate these issues by network densification providing in-band backhauling, thereby enhancing network efficiency and reducing deployment costs [1]. On the other hand, from the physical layer perspective, the concept of a Smart Radio Environment (SRE) is emerging [2], [3]. Here, the environment is no longer a static input but an adaptable and dynamic entity, allowing for dynamic manipulation to improve communication performance. SRE includes two distinct devices, namely Reconfigurable Intelligent Surface (RIS)s and

Network-Controlled Repeater (NCR)s [4], [5]. SRE and IAB are no mutually exclusive; indeed RISs and NCRs can be deployed to improve the communication performance of any generic RAN, including those based on IAB architectures.

RISs are quasi-passive devices that allow controlling the reflection/transmission direction of an impinging electromagnetic (EM) wave by tuning the physical properties of the reflection coefficient of the device itself [6]. At microwaves, RISs are usually manufactured as 2D arrays of unit cells (meta-atoms), whose reflection/transmission coefficient can be dynamically tuned to obtain the desired functionality, following the generalized Snell's law of reflection/refraction [7]. When RISs operate in both reflection and transmission mode, we properly refer to simultaneous transmitting and reflecting RIS (STAR RIS) [8].

Differently, NCRs are active devices that extend traditional amplify and forward relays with proper beamforming capabilities and time-division duplex operation [4]. NCRs are introduced in recent release 18 of the 3rd Generation Partnership Project (3GPP) specifications [9] and are typically made by two analog antenna arrays (panels), one oriented towards the base station (BS) and the other to serve the users in a pre-defined area. Recently, a trisectoral NCR (3SNCR) made by three panels has been introduced to extend the coverage of the conventional two-panel one [10].

The integration of Heterogeneous SRE (HSRE) into future communication networks presents an opportunity to significantly enhance both coverage and overall quality of service (QoS). However, to fully leverage HSRE capabilities, it is crucial to adapt the network planning process, which is the focus of this work. In the following, we review the literature on SRE and HSRE, with a specific emphasis on network planning.

A. Literature on Network Planning within the HSRE

The literature on HSRE comprises works on both RISs and NCRs. For a single transmitting (Tx) – receiving (Rx) pair, the optimal placement of the RIS is explored in works such as [11], [12]. For simplified scenarios, where blockage is not considered, it is preferable to place the RIS either close to the Tx or Rx to reduce the overall path-loss of the cascaded Tx-RIS-Rx link. An example of a RIS deployment strategy is in [11], where the authors analyze a single exemplary geometry of Tx, Rx and RIS, and devise the best relative position of the RIS given its distance from the Tx-Rx baseline. In [12], instead, the authors show that in case the Tx employs a very

This work was partially supported by the European Union - Next Generation EU under the Italian National Recovery and Resilience Plan (NRRP), Mission 4, Component 2, Investment 1.3, CUP D43C22003080001, partnership on “Telecommunications of the Future” (PE00000001 - program “RESTART”)

The authors are with the Department of electronics, Information and Bioengineering, Politecnico di Milano, 20133, Milano, Italy

* These authors contributed equally to this research.

narrow beam (whose projection onto the RIS is smaller than the RIS size), the best RIS deployment is close to the Rx terminal.

A leap forward in the analysis of RIS deployment is in [13], [14], where the authors perform the coverage analysis for a RIS-assisted wireless network, with the aid of stochastic geometry. The former two works aim to yield a stochastic expression of the coverage probability, where BSs, user equipments (UEs), blockers, and RISs might have different stochastic distributions. In [13] it is shown that using RISs results in significant coverage enhancement, particularly when the density of the blockers in space is high. This outcome aligns with similar results obtained in the context of V2V communications [15]. In [14], the authors also consider the effect of interference, showing that as the density of the deployed RISs increases, the power of the desired and interfering signals also increases. In addition to the optimal placement of the RIS, the optimal orientation and phase configuration are analyzed in [16]–[18]. The work [16] extends [11], [12] considering the orientation, while the authors of [17] deal with a coverage range maximization problem considering a STAR RIS. The locations and orientations of multiple indoor RISs to optimize coverage, specifically within shadowed regions without line-of-sight, are discussed in [18].

Concerning NCRs, the available literature is limited. For example, various deployment options for NCRs are discussed in [19], showing increased coverage performance, especially for cell edge UEs. An evaluation of NCR at the system level is reported in [20], which shows that the deployment of NCR must be sensitive to interference, as far as multiple cells are concerned. The comparison between RISs and active relays, such as decode&forward (DF) and amplify&forward (AF), has been addressed in the first literature works, such as [21] and [22]. These works demonstrate that a very large RIS is needed to match the coverage and capacity performance of DF relays, thus the interest is in comparing RISs and AF relays. In [23], RIS and NCR are compared in a simplified illustrative scenario, showing the effect of different beamforming methods and hardware impairment models of the RIS, as well as different parameters of the NCR, such as amplification gain. The aforementioned works (and reference therein) provide insightful guidelines for HSRE planning in simplified scenarios only, where the positions of BSs, UEs and RISs/NCRs are selected without constraints (no buildings, no obstacles, no realistic environments). Therefore, a more realistic planning of the HSRE must take place in real environments. In [24], RISs are compared with NCRs from both the propagation and geometric perspectives, in an urban scenario, where the constraints of buildings and installation are taken into account. The study demonstrates that the preference between RIS and NCR depends not only on their physical capabilities, such as the dimensions of the RIS, the end-to-end amplification gain, and the angular separation between the NCR panels, but also on the geometry of the environment. This work sets the ground for the effective integration of HSRE in large-scale network planning.

From the network planning perspective, few works are available for HSRE. However, comprehensive considerations

for network planning are crucial. A recent study [25] has shown that simply increasing the number of RIS devices does not always lead to proportional performance gains in network coverage, particularly when deployment costs are considered. In [5], the performance of a dense IAB network in the presence of SRE components is evaluated, demonstrating the efficiency of these components in some specific scenarios, such as outdoor sport events. This works calls for an efficient planning approach, but does not focus on it.

In [26], a system-by-design framework is presented to determine the optimal locations and layouts of the minimum number of synthesized passive static metasurfaces to meet coverage requirements in a predefined region of interest. The framework considers a set of candidate sites in realistic urban propagation scenarios for metasurface installation and employs a binary genetic algorithm to decide on the installation sites. However, RISs or NCRs are not considered. Other planning strategies that consider both RISs and relays are in [27], again in a simplified scenario without installation constraints or realistic environment. In [28], a novel mathematical formulation of coverage planning is presented in the RIS-assisted communication problem, which leads to increased throughput and coverage. In [27], an optimal IAB-aided RAN in mmmW is presented, with the aim of enhancing the reliability of the network by determining the best positions and configurations for NCR and RIS. The approach focuses on maximizing the angular separation between the different paths reaching a given candidate site, as well as minimizing the average link length to mitigate blockage [29]. The numerical results confirm that joint installation of both NCR and RIS significantly increases reliability compared to the use of either one alone.

B. Contribution

To address current gaps in network planning for 6G, our previous work [30] introduced the full coverage minimum cost (FCMC) model, which aims to minimize deployment costs while ensuring full area coverage using RIS and NCR components. Building on this foundation, in this paper, we provide a comprehensive approach to network planning within the HSRE, expanding the FCMC model by incorporating additional device types, such as STAR RIS and 3SNCR, along with a new optimization approach, the maximum budget-constrained coverage (MBCC) model, which balances coverage with budget limitations. Using realistic urban maps, precise blockage model and installation constraints, this expanded framework allows for a more accurate analysis of network planning strategies that address both full-coverage and budget-constrained scenarios, making it applicable to diverse urban deployment conditions.

The list of detailed contributions is as follows:

- We consider the precise channel models of RISs and NCRs, accounting for all propagation characteristics, and their physical/geometric limitations. We used a realistic map of the city of Milan for planning purposes. Each HSRE component, given its characteristics, conforms to the layout of the environment. Furthermore, we use cost models in our numerical results for HSRE components that scale with the settings of the components.

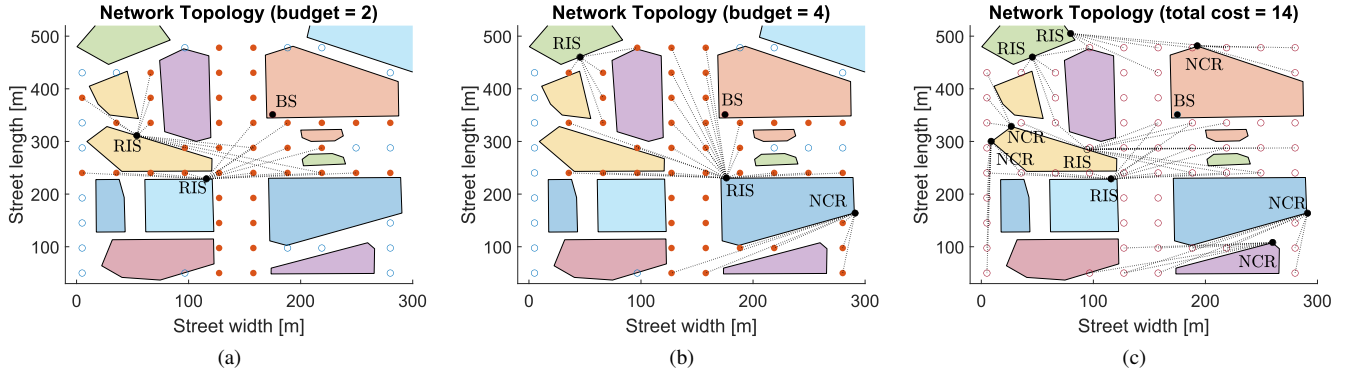


Fig. 1: Network topology with a single fixed BS, RIS and/or NCR devices, achieved with (a) MBCC model, given fixed budget of $B = 2$ units, (b) MBCC model, given fixed budget of $B = 4$ units, and (c) FCMC model. The price of each RIS is assumed to be 1 unit and each NCR is 2 units.

- In addition to already prototyped/deployed components such as RISs and NCRs, we also consider the simultaneous usage of next-generation HSRE components such as STAR RIS and 3SNCR and evaluate their feasibility and effects on performance metrics.
- We provide two mathematical optimization models to minimize the average total cost, given the full coverage of the area considered, namely the FCMC model, and to maximize the coverage percentage, given a fixed budget, namely the MBCC model. The extensive numerical analysis performed by applying the proposed models, allowed us to derive important guidelines on how to configure and deploy HSRE components.

C. Organization

This paper is organized as follows. Section II motivates deploying HSRE in network planning. Section III introduces the system model. In Section IV a detailed description of the components of the SRE with an estimated cost model is discussed. In section V, we formalize the coverage optimization problem, proposing two distinct optimization models. Section VI presents the numerical results and provides insights into deployment strategies, device configurations, and cost analysis. Finally, Section VII concludes the paper.

D. Notation

The bold upper- and lowercase letters represent the matrices and the column vectors, respectively. The (i, j) -th entry of the matrix \mathbf{A} is denoted by $[\mathbf{A}]_{ij}$. Transpose and conjugate transpose of matrix \mathbf{A} are represented by \mathbf{A}^T and \mathbf{A}^H , respectively. The identity matrix of size n is written as \mathbf{I}_n . A complex-valued scalar random variable is denoted by $z \sim \mathcal{CN}(0, \sigma^2)$, where \mathcal{CN} represents the circularly symmetric complex Gaussian distribution. Value of a variable x in dB scale is denoted as $[x]_{\text{dB}}$. The operator $\mathbb{E}[\cdot]$ denotes the expectation, while \mathbb{C} and \mathbb{R} represent the sets of complex and real numbers, respectively. The symbol $\|\cdot\|_F$ represents the Frobenius norm.

II. MOTIVATION

Network planning in the SRE is affected by many parameters. These parameters include configuration and field of view of the devices, static blockers (buildings in our case), geometry of the streets, accurate propagation details of the devices, and overall, the environment. More importantly, the planning depends on how much each of the devices would cost (deployment, scaling, maintenance, or power consumption), and how much budget is available, and what is the optimization goals with related constraints. In this example, Fig. 1 shows a sample network topology for a section of Milan. In this scenario, the configuration and position of a single Base Station (BS) are predefined, while the position and orientation of the SRE devices, RISs and the NCRs, are the focus of optimization. NCRs have an end-to-end amplification gain of 95 dB, and RISs employ 100×100 half-wavelength meta-atoms. The configurations and details of the devices and the optimization model will be discussed exhaustively later in the following sections. Here, each RIS costs 1 units and each NCR costs 2 units. Fig. 1 (a) and Fig. 1 (b), are examples, showing the network topology for the case where we use the MBCC optimization model, whose goal it is to maximize the coverage, when the total available budget is constrained to 2 and 4 units, respectively. Here, the empty circles are the Test Point (TP) that are not covered, while the filled red circles are the TPs that are covered, either via a relay (RIS or NCR), or directly by the BS, or both. The dashed lines show the coverage of TP by the corresponding relaying device. It can be seen that, by changing the available budget, not only the devices used and their number will change, but also their position and orientation will be affected. Increasing the available budget, more TPs can be covered. Instead, in Fig. 1 (c) we use the FCMC optimization model, whose goal is to minimize the total cost, while guaranteeing full coverage of all TPs and, thus, the budget is not limited. It can be seen that the full coverage requirement will not only drastically increase the total cost but will also change the entire network topology, showing how different optimization goals affect planning in SRE.

This example shows how various parameters will be decisive for network planning optimization. Therefore, the goal of the paper is to make a comprehensive consideration of all the effective parameters, as precise as possible, and to propose appropriate optimization models that suit different requirements and goals.

III. SMART RADIO ENVIRONMENT MODEL

Consider the downlink communication shown in Fig. 1, which shows two possible connections, direct and relayed, between a BS and all TP (that stands for possible UEs). The locations of BS, relay, and UE in space, described in a global coordinate system, are indicated as $\mathbf{p}_{BS} = [x_{BS}, y_{BS}, z_{BS}]^T$, $\mathbf{p}_R = [x_R, y_R, z_R]^T$, $\mathbf{p}_{UE} = [x_{UE}, y_{UE}, z_{UE}]^T$, respectively. The set of all potential UE locations is given by $\mathcal{P} = \{\mathbf{p}_{UE}\}$. The BS and the UEs have an antenna array of N_t and N_r elements, respectively.

The relay unit can be either an intelligent metasurface or an NCR. Two types of intelligent metasurfaces are considered: RIS and STAR RIS, depicted in Figs. 2a and 2b, both using M meta-atoms. For NCRs, two configurations are examined: two-panel and 3SNCR, shown in Fig. 2c and 2d, respectively. In the two-panel NCR configuration, the first panel faces the BS, while the second panel faces the coverage area, oriented at an angle α relative to the first panel. Each panel is equipped with N_p antenna elements. In the three-panel NCR configuration, the first panel, which contains N_p antenna elements, is oriented toward the BS, while the other two panels, each with $N_p/2$ antenna elements to comparable complexity. They are positioned so that the angle between each pair of panels is 120° . The antenna arrays have half-wavelength spacing at the carrier frequency $f_0 = c/\lambda$ (for the speed of light c and wavelength λ), while the intelligent metasurface meta-atoms are spaced at $\lambda/4$ intervals.

A. Signal Model

Let $s \in \mathbb{C}$ be the complex symbol to be transmitted, such that $\mathbb{E}[s^*s] = \sigma_s^2$, where σ_s^2 denotes the transmitted power. The transmitted signal is expressed as

$$\mathbf{x} = \mathbf{f} s, \quad (1)$$

where \mathbf{f} denotes the precoding vector, such that $\|\mathbf{f}\|_F^2 = N_t$. The signal transmitted in (1) can be received by the UE directly \mathbf{r}^d , through NCR \mathbf{r}^{NCR} , or via an intelligent metasurface \mathbf{r}^{IM} . This can be expressed as

$$y = \mathbf{w}^H \left(\mathbf{r}^d + \sum_{i \in \mathcal{I}} \mathbf{r}_i^{\text{IM}} + \sum_{j \in \mathcal{J}} \mathbf{r}_j^{\text{NCR}} \right) + \mathbf{w}^H \mathbf{n}, \quad (2)$$

where $\mathbf{n} \sim \mathcal{CN}(\mathbf{0}, \sigma_n^2 \mathbf{I}_{N_r})$ denotes the additive white Gaussian noise, $\mathbf{w} \in \mathbb{C}^{N_r \times 1}$ is the combining vector, and \mathcal{I}, \mathcal{J} denote the set of deployed intelligent metasurfaces and NCRs, respectively.

1) *Direct Signal Model*: The received signal model for the direct link can be expressed as

$$\mathbf{r}^d = \mathbf{H}^d \mathbf{x} \quad (3)$$

with $\mathbf{H}^d \in \mathbb{C}^{N_r \times N_t}$ being the MIMO direct channel.

2) *Relayed Signal Model via Intelligent Metasurface*: The received signal model for the relayed link through an intelligent metasurface can be expressed as

$$\mathbf{r}^{\text{IM}} = \mathbf{H}_o^{\text{IM}} \left(\sqrt{\beta_r} \Phi_r + \sqrt{\beta_t} \Phi_t \right) \mathbf{H}_i^{\text{IM}} \mathbf{x}, \quad (4)$$

where β_r and β_t denote the reflection and transmission coefficient of the intelligent metasurface, respectively, such that $\beta_r + \beta_t \leq 1$, with $\beta_t = 0$ in case the intelligent metasurface is an RIS, and $\beta_t > 0$ for STAR RIS. The reflection and transmission coefficient matrices are denoted by $\Phi_r \in \mathbb{C}^{M \times M}$ and $\Phi_t \in \mathbb{C}^{M \times M}$, $\mathbf{H}_i^{\text{IM}} \in \mathbb{C}^{M \times N_t}$ and $\mathbf{H}_o^{\text{IM}} \in \mathbb{C}^{N_r \times M}$ are the input/output channel matrices between the BS, the intelligent metasurface, and the UE. The reflection/transmission matrix Φ in (4) is diagonal with entries defined as

$$\Phi = \text{diag} \left(e^{j\phi_1}, \dots, e^{j\phi_m}, \dots, e^{j\phi_M} \right), \quad (5)$$

where ϕ_m denotes the phase applied at the m -th element. The phase shifts are assumed to be designed as optimal for every Rx position [31], given the nature of network planning.

3) *Relayed Signal Model via Network Controlled Repeater*: Since the NCR is an active device, the model of the received signal includes the amplified noise. The signal received by the NCR can be expressed as

$$\mathbf{z}^{\text{NCR}} = \mathbf{H}_i^{\text{NCR}} \mathbf{x} + \mathbf{v} \quad (6)$$

where $\mathbf{v} \in \mathbb{C}^{N_p \times 1} \sim \mathcal{CN}(\mathbf{0}, \sigma_v^2 \mathbf{I}_{N_p})$ denotes the noise at the NCR, and $\mathbf{H}_i^{\text{NCR}} \in \mathbb{C}^{N_p \times N_t}$ is the channel matrix between the BS and the NCR. The signal \mathbf{z}^{NCR} in (6) is amplified and forwarded towards the UE. The signal received by the UE through the NCR can be expressed as

$$\mathbf{r}^{\text{NCR}} = \sqrt{g} \mathbf{H}_o^{\text{NCR}} \mathbf{Q} \mathbf{z}^{\text{NCR}} \quad (7)$$

where g denotes the amplification gain, $\mathbf{H}_o^{\text{NCR}} \in \mathbb{C}^{N_r \times N_p}$ denotes the channel matrix between the NCR and the UE. The relaying matrix $\mathbf{Q} \in \mathbb{C}^{N_p \times N_p}$ operates a phase shift between the received signal and the forwarded one. In case the NCR has two panels, the relaying matrix can be expressed as

$$\mathbf{Q} = \mathbf{u} \mathbf{b}^H \quad (8)$$

where $\mathbf{u} \in \mathbb{C}^{N_p \times 1}$ and $\mathbf{b} \in \mathbb{C}^{N_p \times 1}$ denote the forwarding and receiving beamformers, respectively. In the case, the NCR has three panels, the relaying matrix is expressed as

$$\mathbf{Q} = \mathbf{U} \boldsymbol{\xi} \mathbf{b}^H \quad (9)$$

where $\boldsymbol{\xi} \in \mathbb{B}^{2 \times 1}$ is a selection vector that allocates the incoming stream to one of the output panels, and $\mathbf{U} \in \mathbb{C}^{N_p \times 2}$ is a block diagonal matrix, defined as

$$\mathbf{U} = \begin{bmatrix} \mathbf{u}^{(1)} & \mathbf{0} \\ \mathbf{0} & \mathbf{u}^{(2)} \end{bmatrix} \quad (10)$$

with $\mathbf{u}^{(1)} \in \mathbb{C}^{N_p/2 \times 1}$ and $\mathbf{u}^{(2)} \in \mathbb{C}^{N_p/2 \times 1}$ denoting the forward beamforming vectors to each of the output panels, and $\mathbf{0}$ is an $N_p/2 \times 1$ zeros vector.

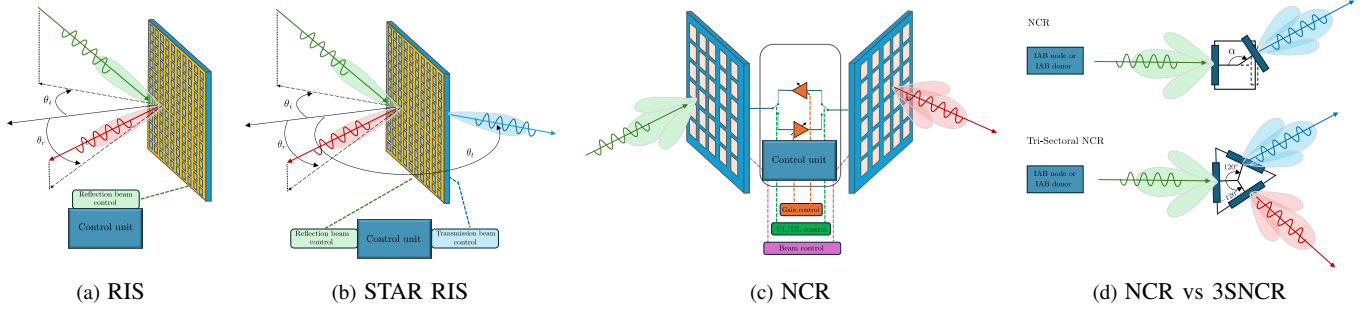


Fig. 2: Illustrative scheme of different SRE components

B. Channel model

This paper assumes a block-fading channel model with independent fading among direct \mathbf{H}^d , forward \mathbf{H}_i , and backward \mathbf{H}_o channels from NCR and intelligent metasurfaces. Considering the challenging propagation conditions at mmWave frequencies, we have adopted the Saleh-Valenzuela cluster-based model [32], in this study. The impulse response of any channel in the model being considered can be expressed as

$$\mathbf{H} = \sum_{p=1}^P \frac{\alpha_p}{\sqrt{P}} \varrho_r(\vartheta_p^r, \varphi_p^r) \varrho_t(\vartheta_p^t, \varphi_p^t) \mathbf{a}_r(\vartheta_p^r, \varphi_p^r) \mathbf{a}_t(\vartheta_p^t, \varphi_p^t)^H, \quad (11)$$

where P is the number of paths, α_p denotes the scattering amplitude of the p -th path, and $\mathbf{a}_t(\vartheta_p^t, \varphi_p^t) \in \mathbb{C}^{N_t \times 1}$ and $\mathbf{a}_r(\vartheta_p^r, \varphi_p^r) \in \mathbb{C}^{N_r \times 1}$ denote the Tx and Rx array response vectors for the p -th path, functions of the Tx and Rx pointing angles $(\vartheta_p^t, \varphi_p^t)$ and $(\vartheta_p^r, \varphi_p^r)$. For convenience, the channel model incorporates the element radiation patterns $\varrho(\vartheta, \varphi)$, which is defined according to [33] for BS, UE, and NCR, while for the intelligent metasurface, it is defined as in [31].

The array factor $\mathbf{a}(\vartheta, \varphi)$ in (11), assuming a uniform planar array, can be expressed as

$$\mathbf{a}(\vartheta, \varphi) = [e^{j\mathbf{k}(\vartheta, \varphi)^T \boldsymbol{\nu}_1}, \dots, e^{j\mathbf{k}(\vartheta, \varphi)^T \boldsymbol{\nu}_L}] \quad (12)$$

where $\mathbf{k}(\vartheta, \varphi) \in \mathbb{R}^{3 \times 1}$ is the wave vector, defined as

$$\mathbf{k}(\vartheta, \varphi) = \frac{2\pi}{\lambda} [\cos(\varphi) \cos(\vartheta), \cos(\varphi) \sin(\vartheta), \sin(\varphi)]^T, \quad (13)$$

and $\boldsymbol{\nu}_\ell = [x_\ell, y_\ell, z_\ell]$ is the position of the ℓ th element of the considered ULA array, expressed in local coordinates.

Having calculated direct or relay channels, instantaneous signal-to-noise ratio (SNR) γ_0 through every link, can be calculated similarly to [24]. The static blockage here is deterministic as we use the actual map of the buildings to form the scenario. The dynamic blockage model is taken from [29], used to calculate the long-term SNR. For instance, for the direct path, the long-term SNR is calculated as [24]

$$\bar{\gamma}^{\text{BS}} = P_B^{\text{BS}} \gamma_0^{\text{BS}} + (1 - P_B^{\text{BS}}) \gamma_0^{\text{BS}}, \quad (14)$$

where P_B^{BS} is the blockage probability of the direct paths, γ_0^{BS} is the SNR when blockage does not happen, while γ^{BS} is the SNR considering the penetration loss or knife edge diffraction [24] [34]. The long-term SNR of the relayed links can be calculated similarly. These long-term SNRs will be used by the

optimization models in the next section. The dynamic blockage probability P_B depends on the length of the considered link, as well as other parameters such as blockers' density, velocity, and dimensions [29].

IV. SRE DEVICES' TECHNOLOGIES AND COSTS

RIS (Fig. 2a) are typically constructed using metasurfaces, which are thin, planar structures composed of sub-wavelength-sized elements. The primary components of an RIS include the sub-wavelength elements and their feed system, each controlled by PIN diodes or varactors, the control circuitry and microprocessors, necessary for dynamic reconfiguration [4]. Based on these, the total cost of a RIS can be divided to the constant deployment and components' cost and variable components' cost scaling linearly with the number of RIS meta-atoms.

One main drawback of RIS is that it can only cover a maximum of half of the plane, that is, the source and destination must be in front of the RIS to be served. A novel alternative to the reflective RIS, is the STAR RIS. The dual functionality of STAR RIS is achieved instead through specialized hardware, often constructed using graphene or multilayered metal patches separated by a polyimide substrate [35] or dielectrics [36]. In the initial prototypes such as in [37] or [38] the independent control of reflection and refraction was not possible and the power is split on both sides of the surface. In more advanced hardware models, more degrees of freedom are available to guarantee the manipulation of the amplitude and phase shift, simultaneously, for transmitted and reflected waves [39]. Independent control for transmission and reflection is enabled by using separate controlling components for the elements in both sides, to manipulate the electric and magnetic currents. This would translate to at least twice more electronic components [40].

NCRs (Fig. 2c) are controlled by base stations to enhance network coverage and performance. Unlike traditional RF repeaters, NCRs act as extensions of the base station, using beamforming and timing synchronization to effectively manage interference and energy consumption. They are transparent to mobile devices and adhere to 3rd Generation Partnership Project (3GPP) standardized procedures for authentication and authorization [41]. NCR employs two panels, each with a uniform planar array (UPA). Both panels can perform beamforming, while the NCR decides also the amplification

TABLE I: Device costs scaling with configurations .

Parameter	Symbol	Value(s)
RIS size	M	$50 \times 50 - 300 \times 300$
NCR gain in dB	$[g]_{dB}$	$30 - 70$
RIS cost per unit cell	O_c^{ris}	6×10^{-5}
NCR deployment cost	O_d^{nocr}	0.8
NCR cost per dB of Gain	O_g^{nocr}	4×10^{-2}
RIS price	O^{ris}	$O_d^{ris} + O_c^{ris} \times M$
STAR RIS price	O^{star}	$2 \times O^{ris}$
NCR price	O^{nocr}	$O_d^{nocr} + O_g^{nocr} \times [g]_{dB}$
3SNCR price	O^{3snocr}	O^{nocr}

gain, and time division duplexing, given the network layer information provided by the BS, an IAB donor or an IAB node, if any IAB architecture is deployed (Fig. 2c). The angular separation between the two panels, to avoid loop-back interference, is one of the main downsides of the NCR, as one panel must face the BS, while the other panel has a limited field of view (FoV). The key cost components of NCRs include beamforming antennas, RF amplifiers, TDD switching units, and the control unit that manages the beamforming and amplification control. Since for a 3SNCR, we consider that the second and third panels have half the number of antennas of a regular NCR, it can be considered that their cost is similar. However, it is expected that an NCR costs much more than a RIS, given that it has power amplifiers and continuous power consumption. Thus, it can be argued that the total cost of a NCR would include site installation and initial component costs (i.e., part of the CAPEX), as well as the cost of operating and maintaining the device (i.e., part of the OPEX).

Based on the above-mentioned considerations, we presume a cost model for the devices as listed in Table I. Similarly to [28], these cost models will be used for networks planning optimization.

Remark: The cost models applied here are rational estimates based on component needs and operational demands. For clarity, prices are presented in units, with a 100×100 RIS taken as the reference, costing 1 unit. Other device prices are scaled relatively to this baseline, emphasizing that in our optimization, it is the relative, not absolute, prices that influence the outcomes. Although actual costs will depend on market conditions and production scales, our framework can seamlessly accommodate updates to these models as vendor data becomes available. Importantly, while variations in the cost model may affect quantitative results, they do not alter the optimization approach, which is agnostic to specific pricing assumptions.

V. COVERAGE OPTIMIZATION

mmWave SRE-based networks are heavily based on deployment geometry, directly impacting their performance, as indicated in previous planning studies [27]. Given large-scale deployments due to the low cost of these devices, understanding the overall impact at the system level is crucial. To accurately assess network performance when these devices are integrated, we employ a Mixed Integer-Linear Programming (MILP) optimization approach. This method guarantees an optimal deployment layout, ensuring that the performance

insights derived represent the best possible outcomes for networks that use these devices. In particular, we employ two different optimization models reflecting complementary network planning objectives, where either the cost is minimized or the coverage is maximized.

A. System Model

Consider a geographic area where the coverage of a pre-deployed BS has to be enhanced by the installation of SRE devices. In particular, let \mathcal{C} be the set of SRE Candidate Sites (CSs). Any $c \in \mathcal{C}$ represents the position in the geographic area where an SRE device can be installed.

As discussed in Sect. III-A, this work considers 4 different types of SRE devices that present a diverse set of performance metrics and costs. As such, the MILP planning approach should be able to select the best SRE device that maximized the planning objective in every active CS. This is mathematically modeled by employing a set \mathcal{D} , which represents the collection of all available SRE technologies to install. The set \mathcal{D} not only allows optimizing network planning by selecting different technologies (RIS or NCR), but also allows the configuration of the selected technology to be further optimized, i.e., RIS size or end-to-end NCR gain. Therefore, its cardinality may be larger than the number of SRE device types.

Let \mathcal{T} be the set of TPs, whose location corresponds to any spatial sampling of the geographic area and can be considered as the positions where the coverage has to be evaluated. We consider a particular TP $t \in \mathcal{T}$ covered when the SNR measured at that location is greater than a parametric threshold Γ . Representing the minimum guaranteed SNR that the optimization will enforce in every TP, Γ is chosen before the planning optimization phase and influences the final network topology.

Nonetheless, the measured SNR is strongly related to the network topology and depends on the BS and the active SRE devices. In particular, any TP $t \in \mathcal{T}$ can be served directly by the BS or indirectly through any SRE device. Let $\bar{\gamma}_t^{\text{BS}}$ be the long-term SNR measured at TP $t \in \mathcal{T}$ limited only to the BS contribution. $\bar{\gamma}_t^{\text{BS}}$ is computed according to the channel model derivations in Sect. III-B. Expressing the minimum SNR requirements into a logical operator, we define the boolean direct link activation parameter

$$\Delta_t^{\text{BS}} = \begin{cases} 1, & \text{if } \bar{\gamma}_t^{\text{BS}} \geq \Gamma \\ 0, & \text{otherwise.} \end{cases} \quad (15)$$

In other words, Δ_t^{BS} is an optimization parameter with value 1 if the BS can guarantee an SNR over threshold for the TP $t \in \mathcal{T}$, and 0 otherwise.

In a similar fashion, we can employ the channel model derivations in Sec. III-B to measure the SNR in every TP for any SRE technology active in any of the CSs, and then compare it with the minimum SNR Γ . We call this quantity $\bar{\gamma}_{t,c}^d$, representing the SNR measured at TP $t \in \mathcal{T}$ limited to the contribution of an SRE device of technology $d \in \mathcal{D}$ installed in CS $c \in \mathcal{C}$.

The result of the comparison operation can be logically expressed by the boolean SRE link activation parameter

$$\Delta_{t,c}^d = \begin{cases} 1, & \text{if } \bar{\gamma}_{t,c}^d \geq \Gamma \\ 0, & \text{otherwise} \end{cases} \quad (16)$$

Notice that Δ_t^{BS} and $\Delta_{t,c}^d$ are called link activation parameters because they inform the optimization model on the possibility of activating a coverage link between the BS or any installed SRE device and a particular TP. Additionally, these parameters can be used to further restrict the coverage link activation. For instance, some Δ_t^{BS} and $\Delta_{t,c}^d$ can be fixed to 0 in case of line of sight obstructions, or to consider other geometric or geographic restrictions.

The proposed model takes into account the cost of employing SRE devices during the network planning optimization phase. In particular, we define as O^d the cost of installing an SRE device of technology $d \in \mathcal{D}$ in the geographic area. As it will be shown in the remainder of this section, the planned network topology can be restricted not to exceed an overall budget, modeled through the parameter B .

B. Full Coverage with Minimum Cost (FCMC)

Building on the system model described above, we now define a MILP formulation for the problem of planning an SRE-empowered wireless network. In particular, the goal of the planning problem is to minimize the cost of the network while guaranteeing minimum coverage (that is, SNR above the threshold Γ) in all TP of the geographic area.

We begin by detailing the decision variables. Let $v_c^d \in \{0, 1\}$ be a boolean decision variable with value 1 if an SRE device of technology $d \in \mathcal{D}$ is installed in CS $c \in \mathcal{C}$ and 0 otherwise. As such, we call v_c^d device installation variable.

We can now give the FCMC formulation:

$$\text{FCMC} \quad \min \sum_{c \in \mathcal{C}, d \in \mathcal{D}} O^d v_c^d \quad (17a)$$

$$\text{s.t.} \quad \Delta_t^{\text{BS}} + \sum_{c \in \mathcal{C}, d \in \mathcal{D}} \Delta_{c,t}^d v_c^d \geq K \quad \forall t \in \mathcal{T} \quad (17b)$$

$$v_c^d \in \{0, 1\} \quad \forall c \in \mathcal{C}, d \in \mathcal{D} \quad (17c)$$

Here, the objective function in (17a) minimizes the overall cost of the network, given as the sum of all the installed SRE devices. Constraint (17b) logically expresses the coverage condition by means of the boolean link activation parameters defined in (15) and (16). For example, assuming $K = 1$, the constraint ensures that every TP experiences SNR above the threshold Γ . If we consider $K > 1$, the network layout is such that every TP will be covered by at least K distinct devices.

Although lean, this formulation is equivalent to a set-cover problem, which is proven to be NP-hard [42]. Nonetheless, heuristic approaches are not required, as large and realistic planning instances can be solved quite quickly, as will be shown in Sect. VI.

C. Maximum Budget-Constrained Coverage (MBCC)

FCMC produces a least-cost network layout where every TP is guaranteed to experience an SNR above threshold Γ . As

an alternative, we also propose the MBCC formulation where the number of covered TPs is maximized (but not guaranteed to be all), with an overall cost constrained to a budget.

MBCC reuses the same notation used in FCMC, with the addition of a coverage boolean decision variable $\nu_t \in \{0, 1\}$ that equals 1 if TP $t \in \mathcal{T}$ is covered (i.e., $\text{SNR} \geq \Gamma$) and 0 otherwise.

$$\text{MBCC} \quad \max \sum_{t \in \mathcal{T}} \nu_t \quad (18a)$$

$$\text{s.t.} \quad \Delta_t^{\text{BS}} + \sum_{c \in \mathcal{C}, d \in \mathcal{D}} \Delta_{c,t}^d v_c^d \geq \nu_t \quad \forall t \in \mathcal{T} \quad (18b)$$

$$\sum_{c \in \mathcal{C}, d \in \mathcal{D}} O^d v_c^d \leq B \quad (18c)$$

$$\nu_t \in \{0, 1\} \quad \forall t \in \mathcal{T} \quad (18d)$$

$$v_c^d \in \{0, 1\} \quad \forall c \in \mathcal{C}, d \in \mathcal{D} \quad (18e)$$

As previously mentioned, the objective in (18a) maximizes the coverage. Constraint (18b) is quite similar to (17a), with the difference that it allows the coverage variables ν_t to be 1 only if the corresponding TP $t \in \mathcal{T}$ can be adequately covered by the BS or by any installed SRE device. Constraint (18c) limits the overall cost of the network to not exceed the budget B .

Note that the MBCC formulation is equivalent to a maximum coverage problem, which is thus NP-hard [42]. However, similarly to FCMC, large instances can be solved with ease.

VI. RESULTS

In this section, we present numerical results obtained using two distinct set of devices: a reduced set and a full set. The reduced set comprises well-established technologies, specifically RIS and NCR, which are already prototyped or deployed in practical networks with known performance characteristics. The full set includes next-generation devices, namely STAR RIS and 3SNCR, in addition to the reduced set. This comparison aims to evaluate whether advanced devices offer substantial performance improvements over conventional options and to assess the trade-offs between performance gains and increased costs. The analysis further underscores the potential benefits of integrating emerging technologies into future networks.

For each scenario, the optimization models are applied to eight different $400\text{m} \times 400\text{m}$ areas within the Milan map, chosen as representative of urban environments. A single BS is placed approximately in the center of each testing area, placed on the roof of a building at a height of 10m. For simplicity, all buildings are assumed to have a uniform height of 6, m due to the unavailability of precise height data. RISs are mounted on the exterior walls of buildings at heights of 5, while NCRs and STAR RISs are installed on the roofs at a height of 6.5, m. Unless otherwise specified, the parameters in Table I are used throughout the simulations.

A. Results with MBCC Optimization Model

This subsection presents numerical results using the MBCC optimization model. Figures 3-(a) and 3-(b) illustrate the

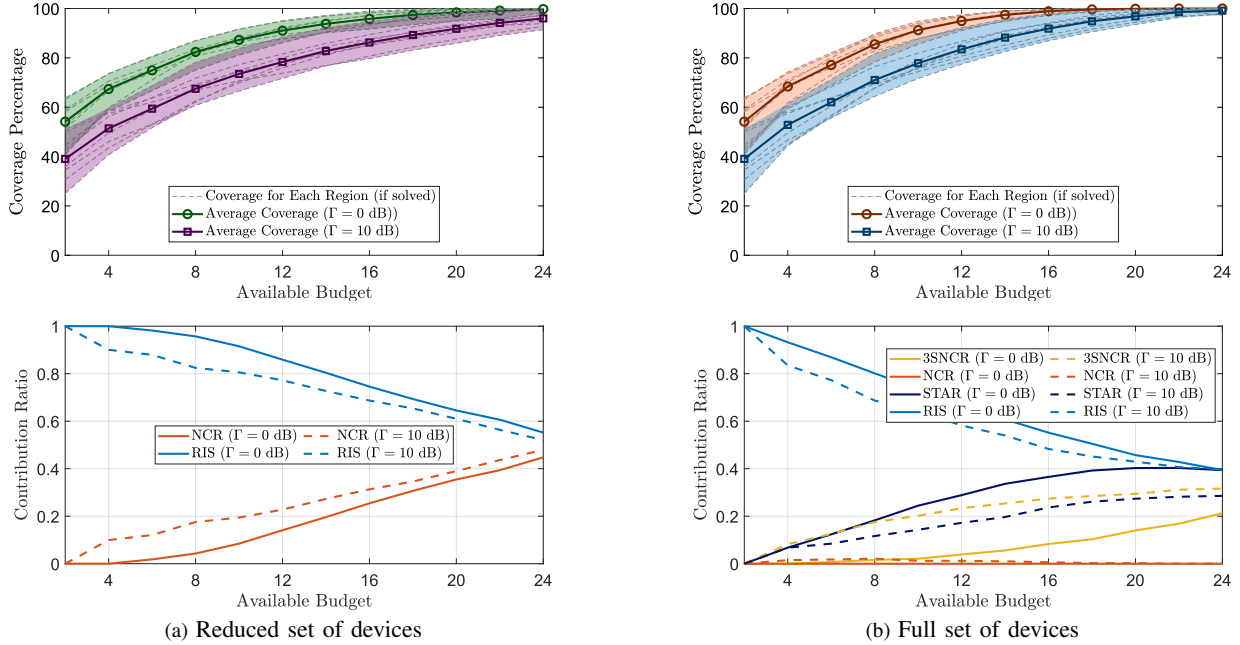


Fig. 3: Average Coverage probability (achieved with MBCC optimization model) vs the total available budget. The used configurations are the default as in Table II.

TABLE II: Default simulation parameters used in Section VI.

Parameter	Symbol	Value(s)
Carrier frequency	f_0	28 GHz
Bandwidth	B	200 MHz
BS Transmit power	σ_s^2	35 dBm
Noise power	σ_n^2	-82 dBm
NCR array size [4]	$N_{p,h} \times N_{p,v}$	12×6
NCR amplification gain [4]	$ g ^2$	55 dB
NCR E2E gain	G	95 dB
NCR noise figure	NF_{ncr}	8 dB
NCR panel separation [24]	α	120 deg
RIS/STAR RIS elements	$M \times M$	100×100
RIS elements's spacing	d_n, d_m	$\lambda_0/2$ m
BS antenna array dimension	N_t	12×16
Tx elements's spacing	d_{Tx}	$\lambda_0/2$ m
BS height [43]	h_{BS}	10 m
UE height	h_{UE}	1.5 m
RIS height	h_{ris}	5 m
STAR and NCR height	h_{star}, h_{ncr}	6.5m
Device prices in default settings	O^{ris}, O^{ncr}	1, 3
Blocker height [29]	h_B	1.7 m
Blocker density [29]	λ_B	$4 \times 10^{-3} \text{ m}^{-2}$
Blocker velocity [29]	V	15 m/s
Blockage duration [29]	μ^{-1}	5 s

maximum coverage percentage as a function of the available budget for the reduced and full sets of devices, respectively. The gray dashed lines represent the results for eight simulated urban regions, while the shaded areas indicate the upper and lower coverage bounds across these regions. The solid lines with markers represent the average values. In each figure, the top panel shows the maximum coverage percentage and the bottom panel shows the contribution ratio, which indicates the relative proportion of each device type among all devices deployed SRE. This representation highlights device behavior and contribution trends under varying budget conditions.

As shown in Fig. 3-(a), the reduced device set demonstrates a clear trend: the contribution of NCRs increases with higher budgets, while the contribution of RISs decreases. This behavior occurs because NCRs, despite their higher cost, effectively serve blind spots behind buildings and distant users due to their amplification gain, overcoming the reflective limitations of RISs. With increasing budgets, the model prioritizes NCRs, a pattern observed for both $[\Gamma]_{dB} = 0$ and $[\Gamma]_{dB} = 10$.

Figure 3-(b) highlights similar trends for the full set of devices, with notable differences. The model favors 3SNCRs over NCRs due to their wider field of view without additional cost. As the budget increases, the contribution of RISs decreases, but instead of relying solely on 3SNCRs, STAR RIS devices play an increasing role. This is because STAR RISs, when placed on rooftops, can serve users behind buildings using refraction, a function that would otherwise require NCRs in the reduced set. With higher budgets, the contribution of STAR RISs continues to increase steadily.

In subsequent analyses, device configurations and costs are scaled to explore their impact. For example, Fig. 4 shows the percentage of coverage versus RIS dimensions, assuming a fixed total budget of $B = 8$ units. This budget can ensure 80% coverage for $\Gamma = 0$ dB, as shown in Fig. 3. As the dimensions of RIS increase from $M = 50 \times 50$ to $M = 300 \times 300$, the coverage percentage initially improves, peaks, and then declines. This behavior suggests an optimal RIS size for coverage.

For example, with the reduced set in Fig. 4-(a) and $[\Gamma]_{dB} = 0$ dB, increasing RIS dimensions up to $M = 120 \times 120$ enhances coverage due to better channel gain. Beyond this point, the increasing cost of larger RISs outweighs their performance benefits, as the additional gain is unnecessary to meet the SNR

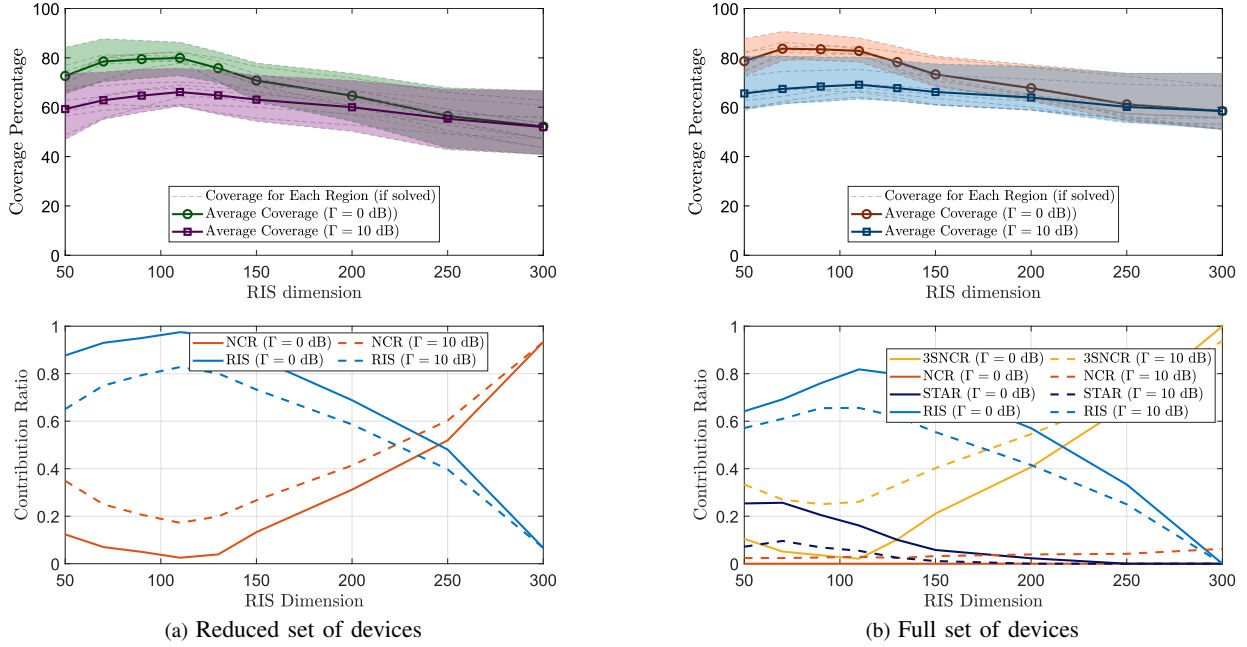


Fig. 4: Average Coverage probability vs RIS dimension, where the total available budget is constrained to $B = 8$ units.

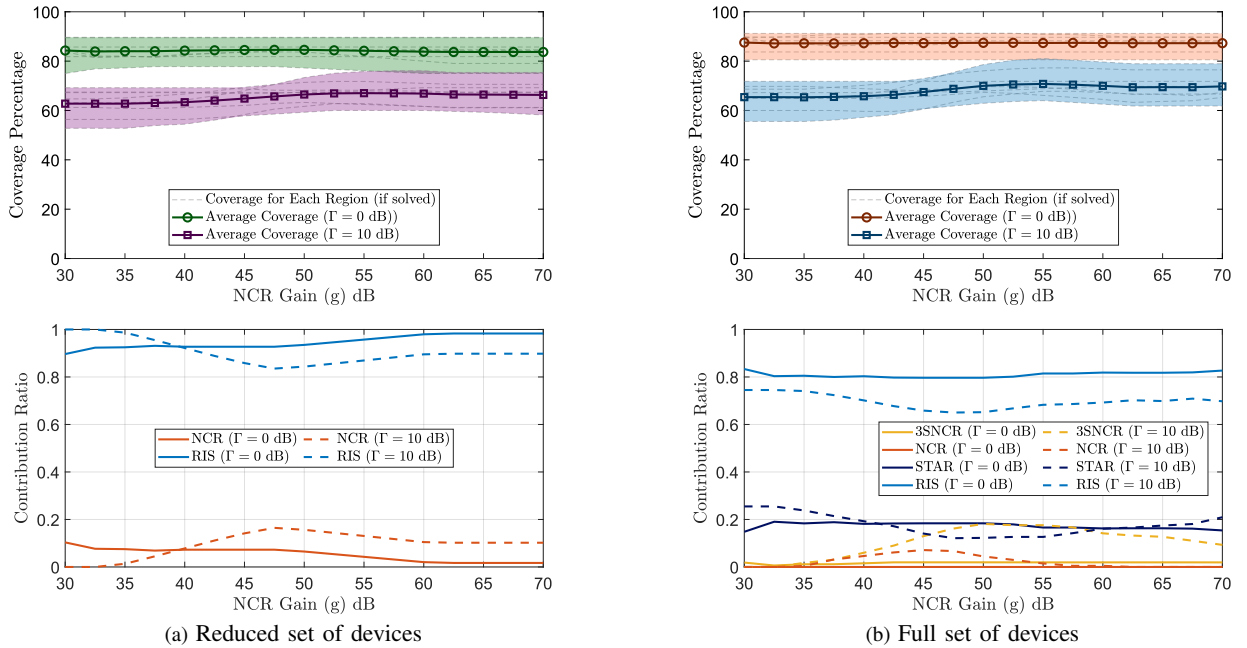


Fig. 5: Average Coverage probability (achieved with MBCC optimization model) vs NCR amplification gain, where the total available budget is constrained to $B = 8$ units. Configurations according to table II.

threshold. A similar trend is evident in the contribution ratio: initially, RIS contributions increase with size but decrease beyond $M = 120 \times 120$, with NCRs or 3SNCRs taking over. In Fig. 4-(b), with the full set of devices, the contributions STAR RIS also decrease as the number of cells in the metasurface increases, indicating that the metasurfaces are effective when their cost is limited.

Figure 5 examines the impact of NCR (or 3SNCR) am-

plification gain on coverage. Here, the configurations of RIS are fixed to the default values of Table II, and the total budget remains $B = 8$ units. For $[\Gamma]_{\text{dB}} = 0$, increasing NCR gain initially reduces their contribution as their cost increases, causing the model to favor RIS or STAR RIS devices, which still satisfy the SNR requirement.

For $[\Gamma]_{\text{dB}} = 10$, the trend differs. Initially, higher NCR gain improves both the coverage percentage and NCR contribution.

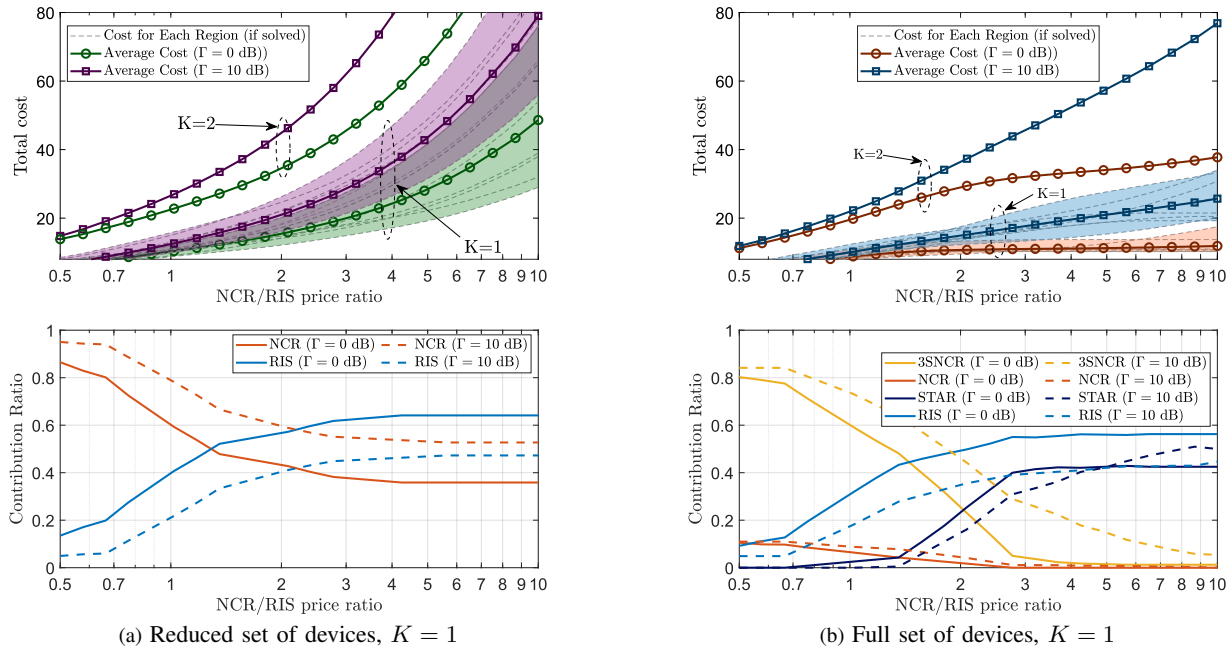


Fig. 6: Average total cost (achieved with FCMC optimization model) vs NCR/RIS price ratio with FCMC optimization model, for fixed settings of RIS/NCR (see table II).

However, beyond amplification gains of $[g]_{\text{dB}} = 47$ for the reduced set (Fig. 5-(a)) and $[g]_{\text{dB}} = 52$ for the full set (Fig. 5-(b)), NCR contributions decline as their costs outweigh their benefits.

B. Results with FCMC Model

In this set of examples, we analyze the performance of the FCMC optimization model, which minimizes the cost required to achieve full coverage of all TPs. Figure 6 shows the total cost as a function of the NCR-to-RIS price ratio for both reduced and full sets of devices. As the price ratio increases, the total cost increases exponentially, particularly with the reduced set of devices (Fig. 6-(a)). This rapid growth occurs because, in this model, all TPs must be covered. TPs far from BS or blocked by buildings can only be served by NCRs in the reduced set, regardless of their cost.

In contrast, the full set of devices (Fig. 6-(b)) mitigates this issue by replacing costly NCRs/3SNCRs with STAR RISs, which can transmit toward TPs behind buildings when placed on the roofs. For $[\Gamma]_{\text{dB}} = 0$, the contribution of RISs surpasses NCRs when the cost ratio exceeds $O^{\text{nrcr}} / O^{\text{ris}} > 1.3$. However, at $[\Gamma]_{\text{dB}} = 10$, the contribution of NCR remains significant even at higher cost ratios, exceeding $O^{\text{nrcr}} / O^{\text{ris}} > 3$, because they achieve higher SNR requirements. With the full set, RISs surpass 3SNCRs when $O^{\text{nrcr}} / O^{\text{ris}} > 1.4$. For $O^{\text{nrcr}} / O^{\text{ris}} > 3$, NCRs/3SNCRs are entirely replaced by RISs and STAR RISs.

Furthermore, Fig. 6 includes results for $K = 2$, where at least two devices serve each TP. As expected, the total cost for $K = 2$ is significantly higher than for $K = 1$. However, the full set of devices helps moderate this increase compared to the reduced set. By setting $K = 2$, the planning becomes

more robust against dynamic blockages that may occur during the online operation of the network.

Similarly to the MBCC model (Section VI-A), we scale the price of the devices based on their configurations (RIS dimension or NCR gain). Initially, the NCR gain is fixed according to Table II, and the RIS configurations are varied. Figure 7 shows the total cost as a function of the RIS dimension \sqrt{M} . For the reduced set of devices (Fig. 7-(a)), increasing the RIS size from $M = 50 \times 50$ to $M = 120 \times 120$ for $[\Gamma]_{\text{dB}} = 0$ and to $M = 150 \times 150$ for $[\Gamma]_{\text{dB}} = 10$, reduces the total cost by approximately 20%. However, beyond these dimensions, the total cost increases due to the increased expense of larger RIS size. For the full set of devices (Fig. 7-(b)), the optimal RIS (or STAR RIS) dimension that minimizes the total cost is approximately $M = 100 \times 100$. Beyond this size, the total cost increases, suggesting that fewer metasurface cells are needed to achieve optimal coverage when advanced devices such as STAR RIS are considered. Remarkably, the total cost of the full set of devices is consistently lower than with the reduced set, and this is due to the greater flexibility in optimizing device deployment with the full set. For certain dimensions, such as $M = 50 \times 50$, the total cost with the full set of devices (Fig. 7-(b)) is 40% lower than with the reduced set (Fig. 7-(a)). These findings align with the results of the MBCC model, confirming the optimal RIS dimensions for cost-effective coverage under a fixed budget.

Fig. 8 examines the impact of NCR amplification gain on total cost, with RIS dimensions fixed to default values. For the reduced set (Fig. 8-(a)), the minimum cost occurs at $[g]_{\text{dB}} = 38$ for $[\Gamma]_{\text{dB}} = 0$ and $[g]_{\text{dB}} = 48$ for $[\Gamma]_{\text{dB}} = 10$. At lower gains, additional NCRs are required to meet SNR requirements, increasing the cost. In contrast, excessively high

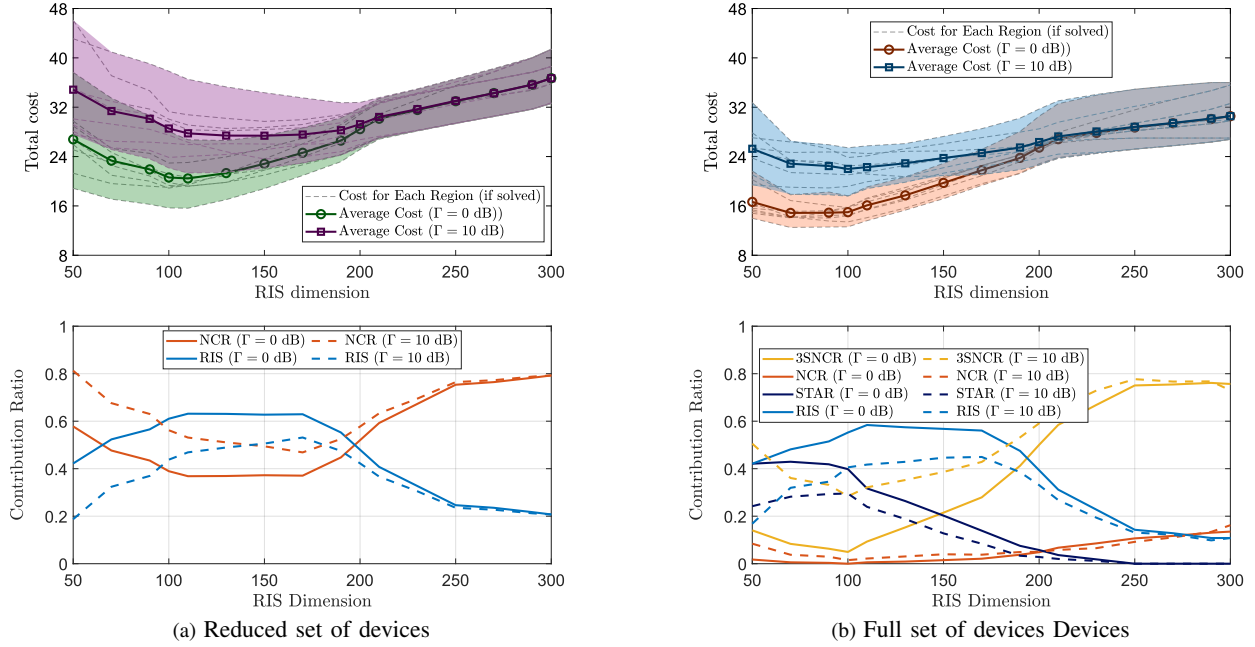


Fig. 7: Average total cost (achieved with FCMC optimization model) vs RIS side size with, where the configurations and price of the NCR is the default according to table II and the cost of the RIS scales according to table I.

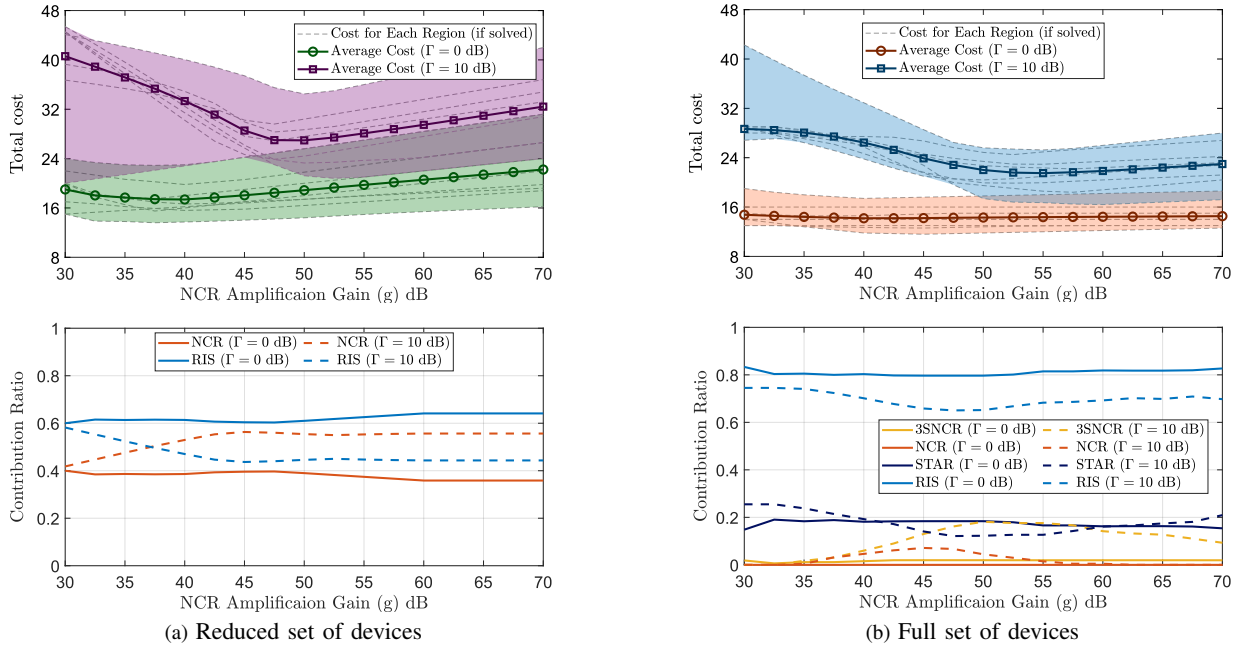


Fig. 8: Average total cost (achieved with FCMC optimization model) vs NCR end-to-end gain (G), where the RIS has default configurations as table II, and the cost of NCR scales according to table I.

gains add unnecessary costs without improving coverage.

The full set of devices (Fig. 8-(b)) exhibits a similar trend, but the total cost is consistently lower due to the flexibility provided by advanced devices. For $[\Gamma]_{\text{dB}} = 10$, the cost reduction can reach 30% for certain NCR gain values. As the gain increases, NCR (or 3SNCR) contributions initially rise but saturate beyond $[g]_{\text{dB}} = 45 - 50$, with additional gain

increases only raising costs without affecting contributions.

Finally, Fig. 9 illustrates the network topology for Piazza Piola in Milan, planned using the FCMC optimization model in different scenarios. The SNR threshold is set to $[\Gamma]_{\text{dB}} = 10$, and the configurations and prices for the NCR (or 3SNCR) devices are fixed according to Table II.

In Fig. 9-(a), only the reduced set of devices is used with

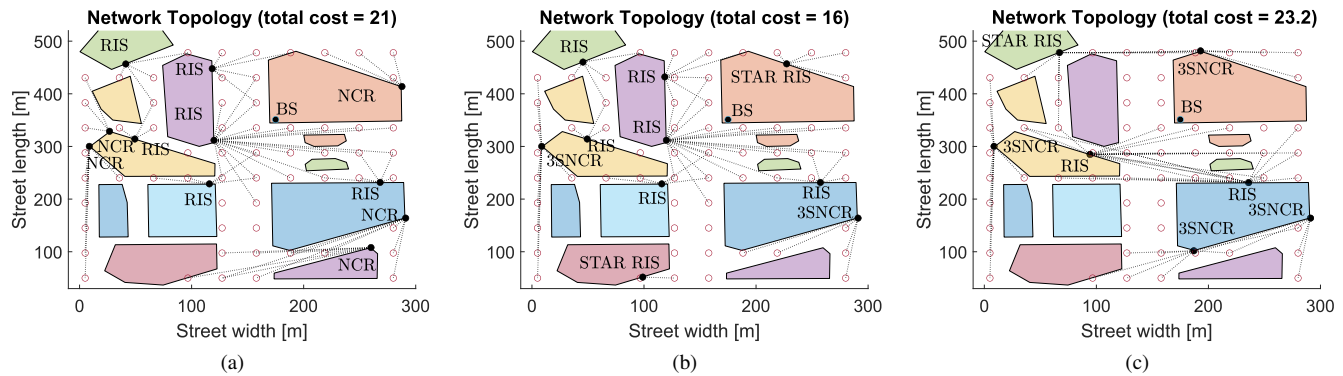


Fig. 9: Network topology, achieved by FCMC optimization model, when using (a) the reduced set of devices with default configurations and prices as in table II (b) full set of devices with default configurations and prices as in table II, (c) full set of devices with RIS dimension $M = 200 \times 200$ and RIS cost scaling according to Table I. The NCR costs and configurations are always assumed default according to table II.

default RIS configurations. In Fig. 9-(b), the full set of devices is employed, again with default configurations for RIS and STAR RIS. The results show a decrease in total cost to 16 units, compared to 21 units with the reduced set. This reduction is achieved by replacing two NCRs with one 3SNCR (as their prices are equivalent) and substituting two additional NCRs with one STAR RIS.

Figure 9-(c) examines the effect of increasing the dimensions of RIS/STAR RIS devices. In this case, the total cost increases due to the higher expense of larger RIS/STAR RIS configurations. As a result, the model shifts to deploy more 3SNCRs compared to Fig. 9-(b), despite the relatively high cost of 3SNCRs. Furthermore, it can be observed that the lengths of the RIS/STAR RIS links are longer in this scenario, as their larger size compensates for increased path loss.

VII. CONCLUSION

In this paper, we develop a deployment optimization framework for HSRE, focusing on realistic urban scenarios. Our study explored both foundational and advanced SRE devices, specifically RIS, STAR RIS, NCR, and 3SNCR. Two optimization models were proposed: one aimed at minimizing the overall cost of complete coverage and another focused on maximizing coverage within a fixed budget.

The numerical results revealed that expanding the selection of the devices to include next-generation technologies such as STAR RIS and 3SNCR provided notable cost efficiency and improved coverage performance. In some scenarios, the integration of these advanced devices achieved up to 40% cost savings compared to the use of traditional devices alone. Moreover, the analysis demonstrated that the optimal choice of devices depends on deployment specifics. RIS is advantageous for cost-effective, broad coverage, while NCR and 3SNCR are essential for boosting signal strength in challenging areas. This flexible planning framework underscores the potential advantages of incorporating emerging technologies into future networks.

REFERENCES

- [1] C. Madapatha, B. Makki, C. Fang, O. Teyeb, E. Dahlman, M.-S. Alouini, and T. Svensson, "On integrated access and backhaul networks: Current status and potentials," *IEEE Open Journal of the Communications Society*, vol. 1, pp. 1374–1389, 2020.
- [2] A. Benoni, F. Capra, P. Da Rù, M. Salucci, G. Oliveri, P. Rocca, and A. Massa, "Smart em environments planning - concepts, advances, and trends," in *2023 17th European Conference on Antennas and Propagation (EuCAP)*, 2023, pp. 1–4.
- [3] M. D. Renzo, A. Zappone, M. Debbah *et al.*, "Smart Radio Environments Empowered by Reconfigurable Intelligent Surfaces: How it Works, State of Research, and Road Ahead," *IEEE Jrn. on Sel. Areas in Comm.*, 2020.
- [4] R. Flamini, D. De Donno, J. Gambini, F. Giuppi, C. Mazzucco, A. Milani, and L. Resteghini, "Towards a heterogeneous smart electromagnetic environment for millimeter-wave communications: An industrial viewpoint," *IEEE Transactions on Antennas and Propagation*, pp. 1–1, 2022.
- [5] G. C. M. da Silva, V. F. Monteiro, D. A. Sousa, D. C. Moreira, T. F. Maciel, F. R. M. Lima, and B. Makki, "Cellular network densification: a system-level analysis with iab, ncr and ris," 2024. [Online]. Available: <https://arxiv.org/abs/2410.02415>
- [6] K. Achouri, M. A. Salem, and C. Caloz, "General metasurface synthesis based on susceptibility tensors," *IEEE Transactions on Antennas and Propagation*, vol. 63, no. 7, pp. 2977–2991, 2015.
- [7] N. Yu, P. Genevet, M. Kats, F. Aieta, J.-P. Tetienne, F. Capasso, and Z. Gaburro, "Light propagation with phase discontinuities: Generalized laws of reflection and refraction," *Science (New York, N.Y.)*, vol. 334, pp. 333–7, 09 2011.
- [8] X. Mu, Y. Liu, L. Guo, J. Lin, and R. Schober, "Simultaneously transmitting and reflecting (star) ris aided wireless communications," *IEEE Transactions on Wireless Communications*, vol. 21, no. 5, pp. 3083–3098, 2022.
- [9] 3GPP, "New wid on nr network-controlled repeaters," 3rd Generation Partnership Project (3GPP), RP 222673, Sep. 2022, TSG RAN meeting no. 97-e, 2022, [Online]. Available: https://www.3gpp.org/ftp/tsg_ran/TSG_RAN/TSGR_97e/Docs/RP-222673.zip (visited on 06/16/2023).
- [10] K. Dong, S. Mura, M. Mizmizi, D. Tagliaferri, and U. Spagnolini, "Advanced tri-sectoral multi-user millimeter-wave smart repeater," 2022.
- [11] Y. Ren, R. Zhou, X. Teng, S. Meng, M. Zhou, W. Tang, X. Li, C. Li, and S. Jin, "On deployment position of ris in wireless communication systems: Analysis and experimental results," *IEEE Wireless Communications Letters*, vol. 12, no. 10, pp. 1756–1760, 2023.
- [12] K. Ntontin, D. Selimis, A.-A. A. Boulogeorgos, A. Alexandridis, A. Tsoilis, V. Vlachodimitropoulos, and F. Lazarakis, "Optimal reconfigurable intelligent surface placement in millimeter-wave communications," in *2021 15th European Conference on Antennas and Propagation (EuCAP)*, 2021, pp. 1–5.
- [13] S. Bagherinejad, M. Bayanifar, M. Sattari Maleki, and B. Maham, "Coverage probability of ris-assisted mmwave cellular networks under blockages: A stochastic geometric approach," *Physical Communication*, vol. 53, p. 101740, 2022. [Online]. Available: <https://www.sciencedirect.com/science/article/pii/S1874490722000805>

- [14] A. H. A. Bafghi, M. Mirmohseni, M. Nasiri-Kenari, B. Maham, and U. Spagnolini, "Stochastic analysis of homogeneous wireless networks assisted by intelligent reflecting surfaces," 2024. [Online]. Available: <https://arxiv.org/abs/2406.07352>
- [15] R. A. Ayoubi, S. Mura, D. Tagliaferri, M. Mizmizi, and U. Spagnolini, "Optimizing curved em skins for opportunistic relaying in vehicular networks," 2024. [Online]. Available: <https://arxiv.org/abs/2405.09730>
- [16] S. Zeng, H. Zhang, B. Di, Z. Han, and L. Song, "Reconfigurable intelligent surface (ris) assisted wireless coverage extension: Ris orientation and location optimization," *IEEE Communications Letters*, vol. 25, no. 1, pp. 269–273, 2021.
- [17] C. Wu, Y. Liu, X. Mu, X. Gu, and O. A. Dobre, "Coverage characterization of star-ris networks: Noma and oma," *IEEE Communications Letters*, vol. 25, no. 9, pp. 3036–3040, 2021.
- [18] J. Zhang and D. M. Blough, "Optimizing coverage with intelligent surfaces for indoor mmwave networks," in *IEEE INFOCOM 2022 - IEEE Conference on Computer Communications*. IEEE Press, 2022, p. 830–839.
- [19] G. C. M. Da Silva, D. A. Sousa, V. F. Monteiro, D. C. Moreira, T. F. Maciel, F. R. M. Lima, and B. Makki, "Impact of network deployment on the performance of ncr-assisted networks," in *2024 19th International Symposium on Wireless Communication Systems (ISWCS)*, 2024, pp. 1–6.
- [20] G. C. M. da Silva, E. R. B. Falcão, V. F. Monteiro, D. C. Moreira, D. A. Sousa, T. F. Maciel, F. R. M. Lima, and B. Makki, "System level evaluation of network-controlled repeaters: Performance improvement of serving cell and interference impact on neighbor cells," 2023. [Online]. Available: <https://arxiv.org/abs/2306.11813>
- [21] E. Bjornson, O. Ozdogan, and E. G. Larsson, "Intelligent reflecting surface versus decode-and-forward: How large surfaces are needed to beat relaying?" *IEEE Wireless Communications Letters*, vol. 9, no. 2, pp. 244–248, 2020.
- [22] Q. Ding, J. Yang, Y. Luo, and C. Luo, "Intelligent reflecting surfaces vs. full-duplex relays: A comparison in the air," *IEEE Communications Letters*, vol. 28, no. 2, pp. 397–401, 2024.
- [23] H. Guo, C. Madapatha, B. Makki, B. Dortschy, L. Bao, M. Åström, and T. Svensson, "A comparison between network-controlled repeaters and reconfigurable intelligent surfaces," 2022. [Online]. Available: <https://arxiv.org/abs/2211.06974>
- [24] R. A. Ayoubi, M. Mizmizi, D. Tagliaferri, D. D. Donno, and U. Spagnolini, "Network-controlled repeaters vs. reconfigurable intelligent surfaces for 6g mmw coverage extension: A simulative comparison," in *2023 21st Mediterranean Communication and Computer Networking Conference (MedComNet)*, 2023, pp. 196–202.
- [25] Z. Li, O. A. Topal, o. T. Demir, E. Björnson, and C. Cavdar, "Mixed static and reconfigurable metasurface deployment in indoor dense spaces: How much reconfigurability is needed?" in *2024 IEEE Wireless Communications and Networking Conference (WCNC)*, 2024, pp. 1–6.
- [26] A. Benoni, M. Salucci, G. Oliveri, P. Rocca, B. Li, and A. Massa, "Planning of em skins for improved quality-of-service in urban areas," *IEEE Transactions on Antennas and Propagation*, vol. 70, no. 10, pp. 8849–8862, 2022.
- [27] E. Moro, I. Filippini, A. Capone, and D. De Donno, "Planning mm-wave access networks with reconfigurable intelligent surfaces," in *2021 IEEE 32nd Annual International Symposium on Personal, Indoor and Mobile Radio Communications (PIMRC)*, 2021, pp. 1401–1407.
- [28] —, "Planning mm-wave access networks with reconfigurable intelligent surfaces," 2021. [Online]. Available: <https://arxiv.org/abs/2105.11755>
- [29] I. K. Jain, R. Kumar, and S. S. Panwar, "The impact of mobile blockers on millimeter wave cellular systems," *IEEE Journal on Selected Areas in Communications*, vol. 37, no. 4, pp. 854–868, 2019.
- [30] R. A. Ayoubi, M. Mizmizi, E. Moro, I. Filippini, and U. Spagnolini, "Advanced network planning in 6g smart radio environments," 2024. [Online]. Available: <https://arxiv.org/abs/2411.06021>
- [31] M. Mizmizi, R. A. Ayoubi, D. Tagliaferri, K. Dong, G. G. Gentili, and U. Spagnolini, "Conformal metasurfaces: a novel solution for vehicular communications," *IEEE Transactions on Wireless Communications*, 2022.
- [32] A. F. Molisch, *Channel Models*, 2011, pp. 125–143.
- [33] 3GPP ETSI TR 138 900, "Study on channel model for frequency spectrum above 6 GHz (version 14.2.0 Release 14)," Jun 2017.
- [34] 3GPP, "Study on channel model for frequencies from 0.5 to 100 ghz (release 16)," 2019.
- [35] X. Wang, J. Ding, B. Zheng, S. An, G. Zhai, and H. Zhang, "Simultaneous realization of anomalous reflection and transmission at two frequencies using bi-functional metasurfaces," *Scientific Reports*, vol. 8, 01 2018.
- [36] T. Cai, G. Wang, S. Tang, H. Xu, J. Duan, H. Guo, F. Guan, S. Sun, Q. He, and L. Zhou, "High-efficiency and full-space manipulation of electromagnetic wave fronts with metasurfaces," *Physical Review Applied*, vol. 8, no. 3, Sep. 2017. [Online]. Available: <http://dx.doi.org/10.1103/PhysRevApplied.8.034033>
- [37] V. Arun and H. Balakrishnan, "RFocus: Beamforming using thousands of passive antennas," in *17th USENIX Symposium on Networked Systems Design and Implementation (NSDI 20)*. Santa Clara, CA: USENIX Association, Feb. 2020, pp. 1047–1061. [Online]. Available: <https://www.usenix.org/conference/nsdi20/presentation/arun>
- [38] H. Zhang, S. Zeng, B. Di, Y. Tan, M. Di Renzo, M. Debbah, Z. Han, H. V. Poor, and L. Song, "Intelligent omni-surfaces for full-dimensional wireless communications: Principles, technology, and implementation," *IEEE Communications Magazine*, vol. 60, no. 2, pp. 39–45, 2022.
- [39] T. Yin, J. Ren, B. Zhang, P. Li, Y. Luan, and Y.-Z. Yin, "Reconfigurable transmission-reflection-integrated coding metasurface for full-space electromagnetic wavefront manipulation," *Advanced Optical Materials*, vol. 12, 08 2023.
- [40] F. Verde, V. Galdi, L. Zhang, and T. J. Cui, "Integrating sensing and communications: Simultaneously transmitting and reflecting digital coding metasurfaces," 2024. [Online]. Available: <https://arxiv.org/abs/2406.10826>
- [41] Pivotal Commware, "Pivot 5G," <https://pivotalcommware.com/pivot-5g/>, [Accessed: June 25, 2024].
- [42] B. Korte and J. Vygen, *Combinatorial Optimization: Theory and Algorithms*, 5th ed. Springer Publishing Company, Incorporated, 2012.
- [43] R. Aghazadeh Ayoubi and U. Spagnolini, "Performance of dense wireless networks in 5g and beyond using stochastic geometry," *Mathematics*, vol. 10, no. 7, 2022. [Online]. Available: <https://www.mdpi.com/2227-7390/10/7/1156>